Characterization of Two-Step Tin-Based Redox System for Thermochemical Fuel Production from Solar-Driven CO2 and H2O Splitting Cycle

ARTICLE *in* INDUSTRIAL & ENGINEERING CHEMISTRY RESEARCH · APRIL 2014

Impact Factor: 2.59 · DOI: 10.1021/ie500206u

4 AUTHORS, INCLUDING:

Gael Leveque
École Polytechnique Fédérale de Lausanne
7 PUBLICATIONS **27** CITATIONS

I&EC research
Industrial & Engineering Chemistry Research

Article

pubs.acs.org/IECR

Characterization of Two-Step Tin-Based Redox System for Thermochemical Fuel Production from Solar-Driven CO_2 and H_2O Splitting Cycle

Gaël Levêque,[†] Stéphane Abanades,*[,†] Jean-Claude Jumas,[‡] and Josette Olivier-Fourcade[‡]

[†]Processes, Materials, and Solar Energy Laboratory, PROMES-CNRS (UPR 8521), 7 Rue du Four Solaire, 66120 Font-Romeu, France

[‡]Institut Charles Gerhardt (UMR 5253), Université Montpellier 2, Place E. Bataillon, 34095 Montpellier Cedex 5, France

ABSTRACT: The solar thermochemical dissociation of H_2O and CO_2 for renewable fuel production from two-step SnO_2/SnO cycle is considered. This cycle is based on the solar production of SnO phase in a first endothermic step that is subsequently used for splitting CO_2 and H_2O in a second exothermic step. The reactivity of tin-based species was studied in order to elucidate the phenomena occurring during its heating and subsequent reoxidation in a H_2O or CO_2 atmosphere to produce H_2 or CO. Two main types of reactant were considered for comparing their reactivity: SnO nanopowder obtained via solar sublimation and condensation of commercial SnO powder, and Sn/SnO_2 nanopowder obtained via disproportionation of nanosized SnO. The reaction rate was quantified via thermogravimetry analysis and the reaction products were characterized using Mössbauer spectrometry and X-ray diffraction. The SnO and Sn/SnO_2 nanopowders are more reactive with H_2O than with CO_2 in the range 550−650 °C. SnO is also more reactive with oxidants than Sn/SnO_2. The disproportionation reaction starts significantly around 600 °C, giving rise to a particular Sn^{II} phase that reacts faster with the oxidants but is more prone to passivation. A kinetic study yields an activation energy of 101 ± 10 kJ mol^{-1} and 53 ± 1 kJ mol^{-1} for the Sn/SnO_2 oxidation with CO_2 and H_2O, respectively.

1. INTRODUCTION

Carbon-free hydrogen and synthetic fuels production from concentrated solar energy (so-called solar fuels production) is a major strategic stake for climate change mitigation and fossil fuel substitution by sustainable energy vectors. Contrary to electrochemical processes, thermochemical processes using metallic redox pairs make direct use of high-temperature heat to drive the endothermic reaction, thus potentially resulting in a higher hydrogen production efficiency compared to electrolysis that is limited by the heat-to-electricity conversion.

Among the feasible routes toward solar fuels,[1,2] the splitting of H_2O and CO_2 via two-step thermochemical cycles based on metal oxide redox couples are foreseen as a long-term possible solution by advantageously eliminating the use of fossil fuels and the associated CO_2 emissions.[3,4] The main scope of the process relates to the solar thermochemical reduction of CO_2 and H_2O for the generation of CO and H_2 as high-value solar fuels that can be further processed to carbon-neutral liquid fuels.

In particular, a process based on the SnO_2/SnO redox pair has been developed at the PROMES laboratory.[5−10] It is composed of two steps: (1) a high-temperature solar powered thermal reduction of SnO_2 to $SnO_{(g)}$ (eq 1) and (2) a low temperature reoxidation in H_2O/CO_2 atmosphere, yielding the initial stannic oxide and H_2/CO (eq 2).

$$SnO_2\ (s) \rightarrow SnO\ (g) + 0.5O_2 \quad (1)$$

$$SnO\ (s) + \frac{H_2O}{CO_2} \rightarrow SnO_2\ (s) + \frac{H_2}{CO} \quad (2)$$

A particularity of this system is that the reduced species (stannous oxide) is obtained by SnO vapor condensation, yielding a nanosized powder with a high specific surface area beneficial to the second step. The cycle proceeds in the same way as the two-step ZnO/Zn cycle in which gaseous Zn is first produced from ZnO solar thermal dissociation, and the condensed Zn nanopowder then reacts with H_2O and/or CO_2 to produce the fuel and ZnO that can be recycled to the solar step.[11,12] The main advantage of the SnO_2/SnO system over ZnO/Zn is the higher thermal dissociation yield during the solar step above 1600 °C, because the backward recombination reaction was shown to be more pronounced in the case of ZnO than SnO_2 dissociation.[13]

The reactive nanopowder produced during the solar thermal reduction is never pure SnO but rather a mix of SnO_2 and SnO because of the partial recombination of SnO and O_2, which depends on the reaction conditions (temperature, pressure, cooling rate). Depending on its composition, the mix is predicted to evolve differently with temperature, which results in different mixed phases (Figure 1, from[14]). In particular, the disproportionation reaction (eq 3) is most likely to occur, with a risk of partial melting of the powder that would decrease the specific surface of the powder (and thus its reactivity) by enlarging the grain size.

$$2SnO \rightarrow SnO_2 + Sn\ (l),\ \Delta G_{298K} = -9.11\ kJ/mol \quad (3)$$

Various studies exist concerning stannous oxide disproportionation, with a variety of results underlining the dependence

Received: January 15, 2014
Revised: March 14, 2014
Accepted: March 17, 2014

   dx.doi.org/10.1021/ie500206u | *Ind. Eng. Chem. Res.* XXXX, XXX, XXX−XXX

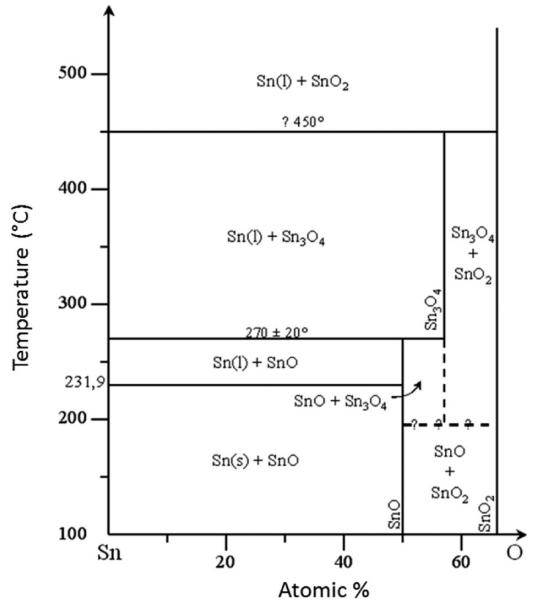

Figure 1. Sn−O phase diagram.

on the SnO preparation. A common result is the observation of an intermediate and metastable phase, a mixed oxide (Sn_2O_3[15,16] or Sn_3O_4[17−20]) containing both Sn^{II} and Sn^{IV}. Moreno et al.[19] studied the decomposition of SnO at 450 °C by Mössbauer spectroscopy and found an intermediate species identified as Sn_3O_4. It contains a particular Sn^{II} phase (isomer shift δ 2.58 mm s^{-1}, quadrupole splitting Δ = 2.01 mm s^{-1}), different from Sn^{II} constituting SnO. Accumulation of the intermediate is observed in the 100−1000 min time range.

Giefers et al.[16] studied SnO powder disproportionation using X-ray diffraction with synchrotron radiation in the 300−550 °C range and report the production of a Sn_2O_3 intermediate, which depends highly on the synthesis method of SnO (results differ for two powders of similar size and composition, but manufactured by two different companies), and on the particle size (less intermediate is produced from the ground sample). This supports an Avrami−Erofeyev solid-state chemical mechanism (nucleation and growth mechanism), where the reaction is limited by the nucleation rate. Then, the use of fine particles should restrict the growth of the nuclei to smaller grains and thus reduce the total reaction rate because each small grain needs its own nucleus, when the progress of the reaction is much faster than the nucleation rate. There is, however, no available information concerning this reaction for submicrometer particles, in particular SnO nanopowders.

From these studies arise two major concerns when using SnO for thermochemical H_2O/CO_2 splitting: (i) Competition between disproportionation and reoxidation with H_2O or CO_2 is most likely to occur during SnO heating up to the oxidation temperature, which may modify the material composition and reactivity, depending on the time and the temperature. The reactivity of the intermediate metastable tin oxide that can appear is not known. (ii) The actual evolution of a nanosized solar-produced SnO powder is unknown since both the synthesis method involving SnO vapor condensation and the resulting particle size are very particular.

The present study aims at clarifying the evolution of the speciation of a SnO solar nanopowder as a function of the temperature and at evaluating its influence on the subsequent oxidation reaction with CO_2 and H_2O. ^{119}Sn Transmission Mössbauer Spectroscopy (TMS) was appropriate to determine precisely the oxidation state and speciation of Sn atoms, and the oxidation rate of different tin-based compounds was investigated via thermogravimetry analysis (TGA) to elucidate and compare the reaction mechanism.

2. MATERIALS SYNTHESIS

Various tin-based materials were prepared and subjected to different treatments. SnO nanopowder was first produced by Solar Physical Vapor Deposition (SPVD) of commercial SnO (Sigma Aldrich, >97% purity). Part of this powder was subjected to complete disproportionation (for 20 min at 680 °C) in order to produce an equimolar mixture of Sn and SnO_2 (in which only Sn can be oxidized) with a similar particle size compared to the initial SnO nanopowder, as confirmed by electron microscopy observations. Although particle growth was observed, the size remained on the same scale. This means that the simultaneous SnO_2 formation prevents the tin

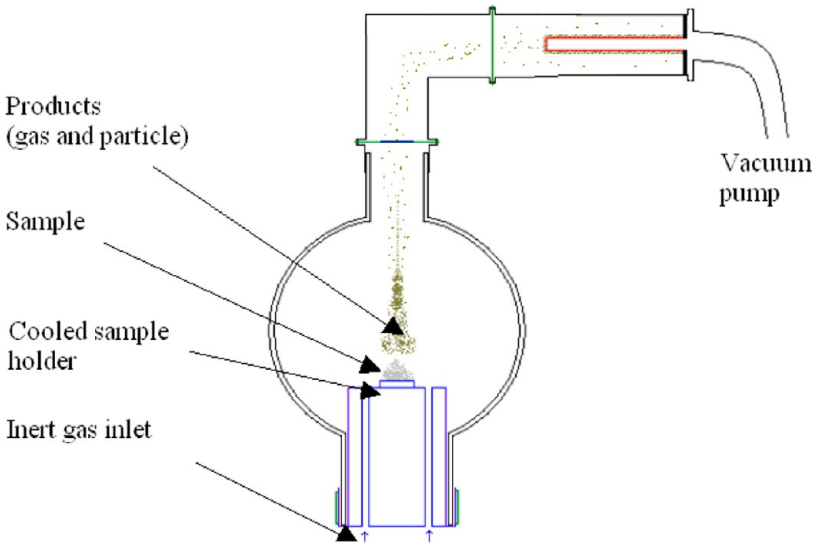

Figure 2. Schematic of the solar reactor for the synthesis of SnO nanopowder from either SnO_2 thermal reduction or SnO sublimation-condensation.

dx.doi.org/10.1021/ie500206u | Ind. Eng. Chem. Res. XXXX, XXX, XXX−XXX

agglomeration that could result in a drastic particle size increase. Note that this method for Sn synthesis was chosen because it is actually not possible to synthesize pure Sn as a nanopowder via SPVD due to the low melting point of metallic tin (232 °C) and its high boiling point (2602 °C). In addition, SnO samples were also produced via solar thermal reduction of commercial SnO_2 (Merck, 99% purity). Finally, commercial SnO and synthetic SnO with micrometer-size particles were also used for results comparison. Then, the materials reactivity during oxidation in H_2O or a CO_2 atmosphere was investigated and compared. ^{119}Sn TMS and XRD were used to determine the Sn speciation in the various samples.

2.1. Experimental Setup for Synthesis of SnO Nanopowders. The synthesis of SnO involving either SnO_2 thermal reduction or SnO sublimation-condensation was performed in a solar reactor[13] (Figure 2) placed at the focal point of a parabolic concentrator (2-m-diameter, 0.85 m focal distance, maximum flux density of 16 MW/m^2 with a Gaussian distribution). The setup is composed of a water-cooled sample holder subjected to the concentrated solar radiation. A transparent glass vessel surrounds the irradiated zone to provide airtightness of the reactor while letting the concentrated solar rays to pass through. Inert gas sweeping and particles transport is ensured by an annular gas inlet around the sample holder and a vacuum pump located at the outlet. The neutral gas flow ensures both the sheathing and cooling of the updraft particle flow. The reactor was operated at reduced pressure (200 ± 20 hPa) in a neutral atmosphere (1 NL/min of N_2). It is settled at the focal point of the parabola that concentrates on a 12-mm-diameter area the solar flux reflected by a 2 × 2 m^2 heliostat. Once the necessary temperature is reached (over 1400 °C for SnO_2 thermal reduction; sublimation of commercial SnO starts earlier), a plume of $SnO_{(g)}$ forms and condenses rapidly due to the temperature drop and then deposits on the upstream filter. A controlled trap-door allows adjusting the incoming solar flux density, which is twice lower for SnO sublimation than for SnO_2 thermal reduction. Once the sample is consumed, the reactor is slightly overpressured in order to remove the filter, and the powder is recovered (under an inert atmosphere or air).

2.2. SnO and Sn Oxidation with H_2O/CO_2 for H_2/CO Production. The reactivity of the synthesized samples (SnO and SnO_2/Sn nanopowders) was studied by using a TGA apparatus (Setaram Setsys Evolution) under isothermal and nonisothermal conditions in the presence of CO_2 (CO_2 mole fraction of 50%, total flow rate of 20 mL min^{-1}) and/or H_2O (40 mL min^{-1} of argon with 80% RH at 40 °C, i.e., 1.6 mg min^{-1} of water, steam mole fraction of 5%) at atmospheric pressure. For isothermal TG, the sample was first heated in Ar up to the targeted reaction temperature (20 K/min) and the gaseous reactant (CO_2 or H_2O) was then injected once the sample temperature was reached, whereas it was injected during sample heating at controlled heating rates during nonisothermal TG. The reactant powder (about 20 mg) was placed in an alumina crucible and subjected to the suitable temperature program and gas atmospheres. The chemical conversion was calculated dynamically from the time-dependent sample mass variation (sample oxidation) to quantify the reaction progress.[21] The main reactant was SnO nanopowder obtained via SPVD of commercial SnO or Sn/SnO_2 obtained after SnO disproportionation at 680 °C for 20 min in an argon flow. Complete disproportionation was confirmed by using Mössbauer spectrometry and XRD analysis, and the formation of droplets was not observed (only a change in color from light brown to light gray).

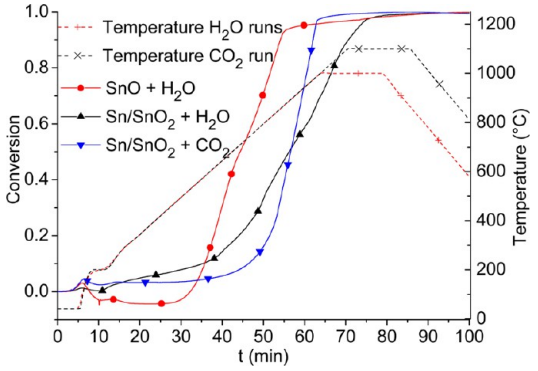

Figure 3. Oxidation of SnO and Sn/SnO_2 nanopowders during nonisothermal TG runs in the presence of CO_2 or H_2O.

3. RESULTS AND DISCUSSION

3.1. Reactivity of SnO and Sn with H_2O and CO_2. Nonisothermal TG runs with a constant heating rate (15 K min^{-1}) were first performed to evaluate the temperature of the reaction start and the temperature of complete conversion (Figure 3). H_2O and CO_2 were continually injected during temperature rise (H_2O was injected from 200 °C and CO_2 was injected from 100 °C). The reaction was always complete at the end of the nonisothermal TG runs, and the global mass increase due

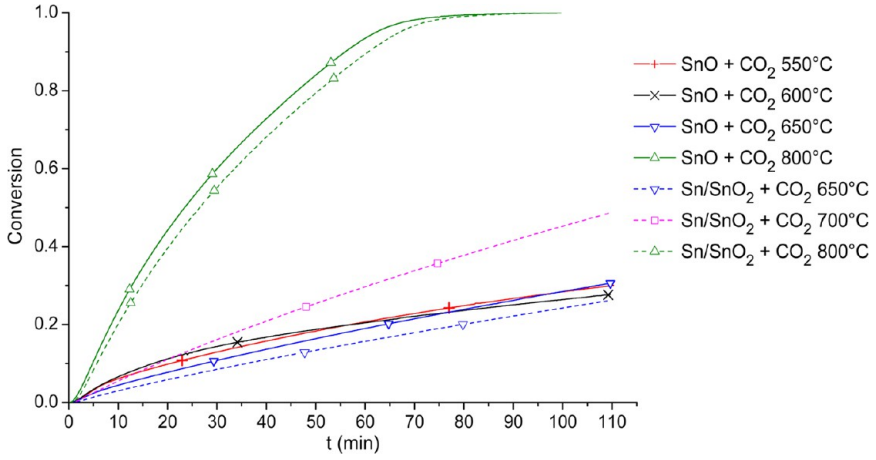

Figure 4. Oxidation of SnO and Sn/SnO_2 nanopowders during isothermal TG runs in a CO_2 atmosphere.

dx.doi.org/10.1021/ie500206u | Ind. Eng. Chem. Res. XXXX, XXX, XXX−XXX

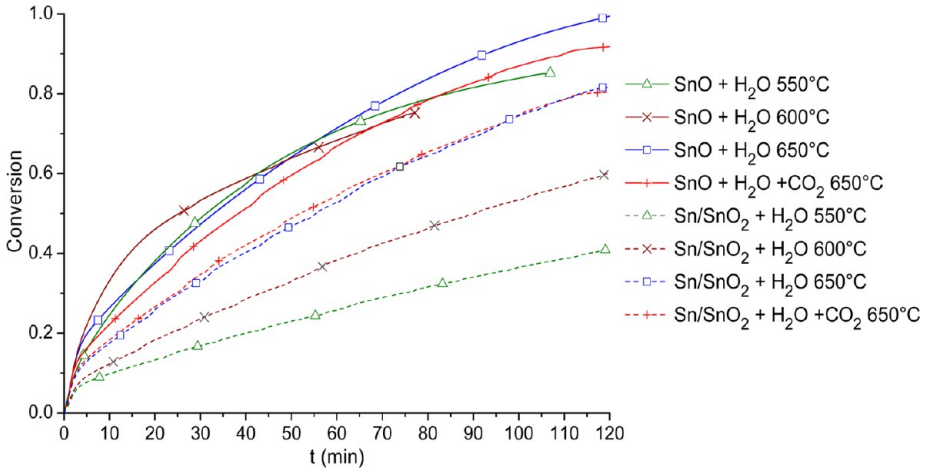

Figure 5. Oxidation of SnO and Sn/SnO_2 nanopowders during isothermal TG runs in a H_2O atmosphere.

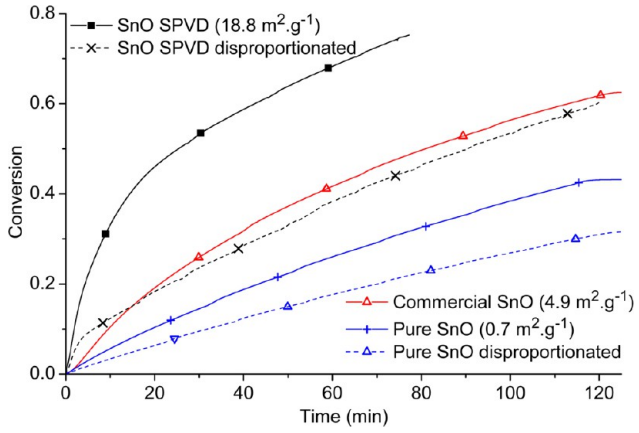

Figure 6. Comparison of SnO powders reactivity during oxidation at 600 °C in a H_2O atmosphere.

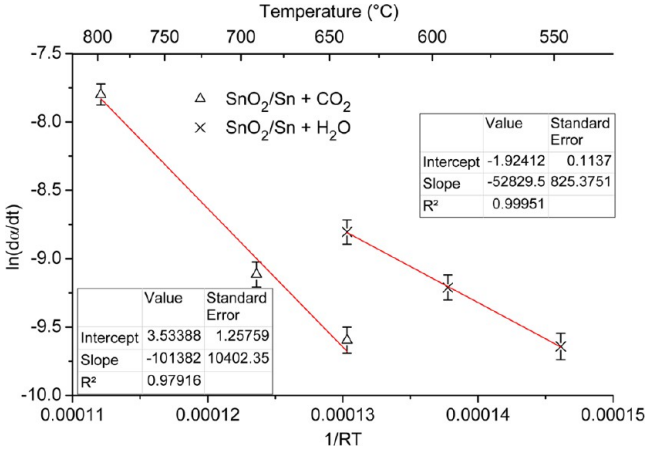

Figure 7. Linear regression of the logarithm of reaction rate versus temperature for Sn oxidation with H_2O and CO_2.

to sample oxidation (oxygen uptake) was used to determine the initial mass fraction of SnO reactant in the powder (73 ± 2% mass).

For Sn/SnO_2 (obtained from SnO disproportionation) reacting with H_2O, the sample weight starts to increase as soon as vapor is injected at 200 °C, but the reaction rate increases moderately with the temperature. The reaction rate of Sn oxidation with H_2O then increases significantly from

Table 1. Common Reaction Mechanisms

mechanism	symbol	$f(\alpha)$
phase boundary controlled reaction (2D)	R2	$(1-\alpha)^{1/2}$
unimolecular decay law	F1	$(1-\alpha)$
nucleation and growth	A2	$2(1-\alpha)[-\ln(1-\alpha)]^{1/2}$
diffusion (3D)	D3	$((3(1-\alpha)^{2/3})/(2[1-(1-\alpha)^{1/3}]))$

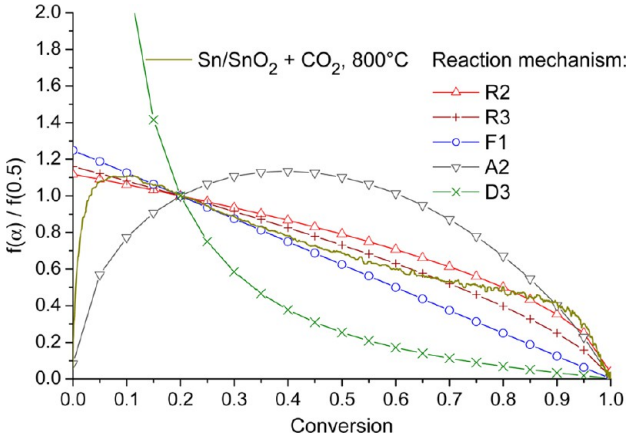

Figure 8. Master plot analysis for Sn/SnO_2 oxidation with CO_2.

650 °C. Sn oxidation with CO_2 only starts from 600 °C, and the weight gain follows a linear and steeper trend above 700 °C. In contrast, the oxidation reaction with H_2O starts promptly at 420 °C for the untreated SnO, but the steepness of the conversion curve diminishes slightly above 650 °C because of SnO disproportionation. Therefore, Sn is the main species that reacts at higher temperatures (over 650 °C).

Isothermal oxidation runs were then carried out to highlight the influence of the disproportionation process on the oxidation with CO_2 (Figure 4) and H_2O (Figure 5). While both the reaction rate and the final conversion increase with the temperature (from 650 to 800 °C) for Sn/SnO_2, only the conversion versus time profile evolves between 550 and 650 °C for SnO, but the final SnO conversion is not changed significantly (for both CO_2 and H_2O). This temperature domain corresponds to the favorable conditions for disproportionation. The SnO oxidation reaction initially proceeds faster at 600 °C than at 550 or 650 °C regardless of the oxidizer (H_2O or CO_2), but the reaction rate then decreases and the final conversion is

dx.doi.org/10.1021/ie500206u | Ind. Eng. Chem. Res. XXXX, XXX, XXX−XXX

lower at 600 °C than at 550 or 650 °C. This reactivity decrease with time is presumably the result of the prevailing reacting species that shifts from SnO to Sn formed from the concomitant disproportionation reaction. Note that the oxidation rates of SnO and Sn/SnO_2 with CO_2 at 800 °C are very similar (Figure 4), which confirms the complete disproportionation of the SnO during the temperature rise in argon before CO_2 injection. For a given temperature (in the range of 550−650 °C), the oxidation rate of SnO is higher than that of Sn/SnO_2. Finally, the oxidation rate of SnO and Sn/SnO_2 with a mixture of H_2O and CO_2 fed simultaneously does not show any significant change when compared to the reaction rate with H_2O only (Figure 5), which denotes a negligible CO_2 conversion.

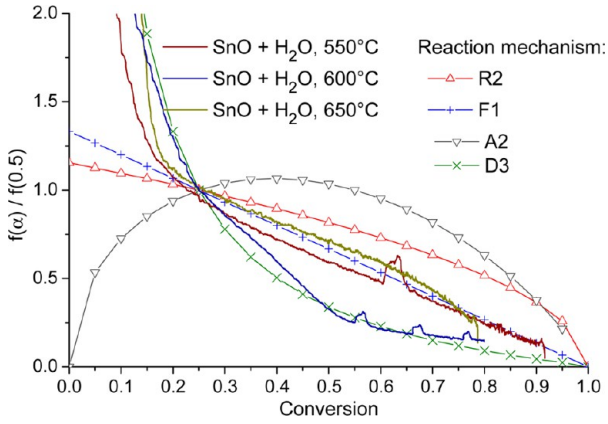

Figure 9. Master plot analysis for SnO oxidation with H_2O.

The oxidation rates obtained during oxidation of SnO SPVD are consistent with previous results obtained with SnO synthesized by solar thermal reduction of SnO_2,[21] which points out similar morphology/reactivity and proves that the SnO nanopowder obtained via solar sublimation-condensation of commercial SnO is representative of the real solar powder obtained from SnO_2 thermal reduction.

Finally, the reactivity of raw commercial SnO (Sigma Aldrich, >97% purity) and synthetic pure SnO produced from $SnCl_2$ aqueous precipitation (purity checked through XRD and Mössbauer spectroscopy) was investigated for comparison with the reactivity of the solar-produced nanopowders (Figure 6). The main varying characteristics are the specific surface area and the particle size (respectively 0.2 and 1.4 μm for commercial and synthetic SnO and 54 nm for SnO SPVD, estimated from BET measurements). The reaction rate and chemical conversion are substantially improved when using solar-produced powders compared to micrometer-sized particles (for both SnO and Sn/SnO_2 obtained via SnO disproportionation). Indeed, the higher specific surface area increases the oxidation kinetics, and the large surface-to-volume ratio offered by small particles favors their oxidation and alleviates surface passivating effects encountered with micronic particle size. Consequently, the interest of using solar-produced SnO particles for improving the reactivity is evidenced.

In any case, the reactivity of Sn obtained from SnO disproportionation was found to be lower than the reactivity of SnO and Sn^{II} species. This explains why the SnO oxidation rate with H_2O and CO_2 decreases with time. The concomitant SnO disproportionation forms Sn and SnO_2. From a chemical viewpoint, the SnO_2 can be considered inert, but the presence of SnO_2 nanoparticles around the Sn particles may hinder the access

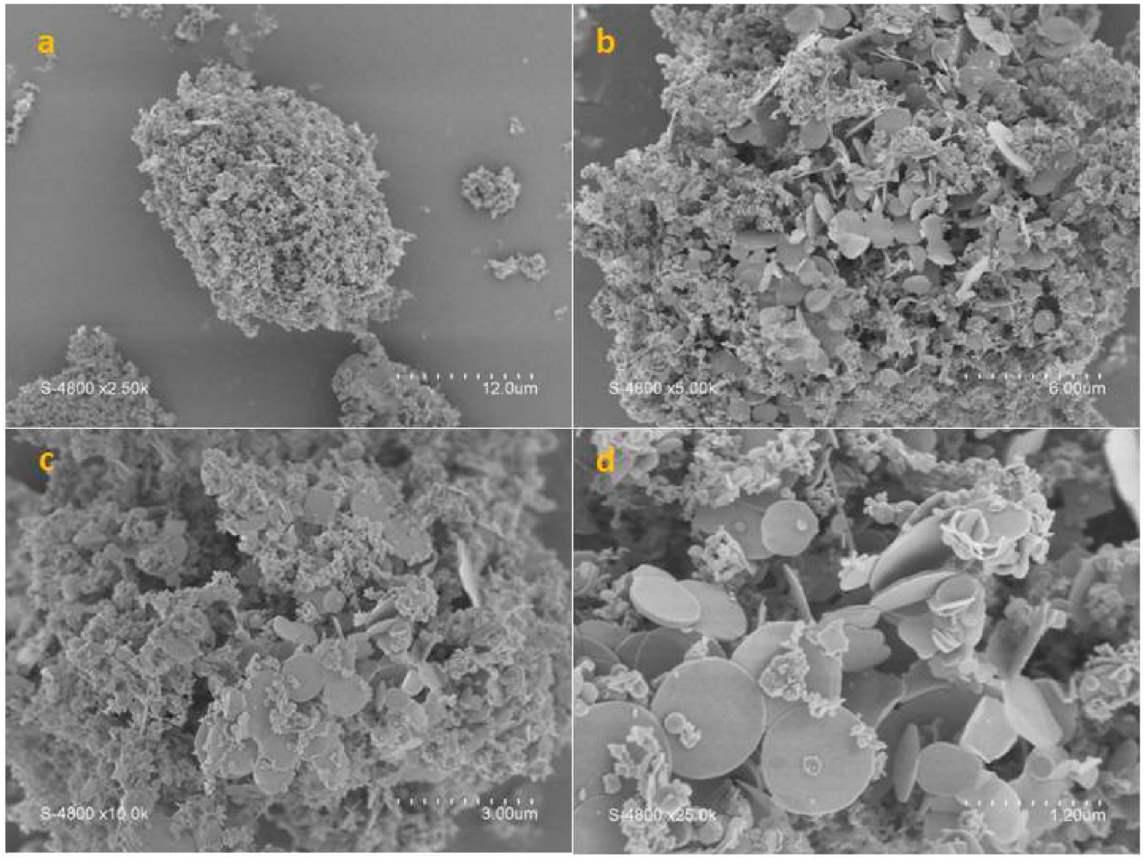

Figure 10. SEM imaging of SnO produced via SPVD.

dx.doi.org/10.1021/ie500206u | Ind. Eng. Chem. Res. XXXX, XXX, XXX−XXX

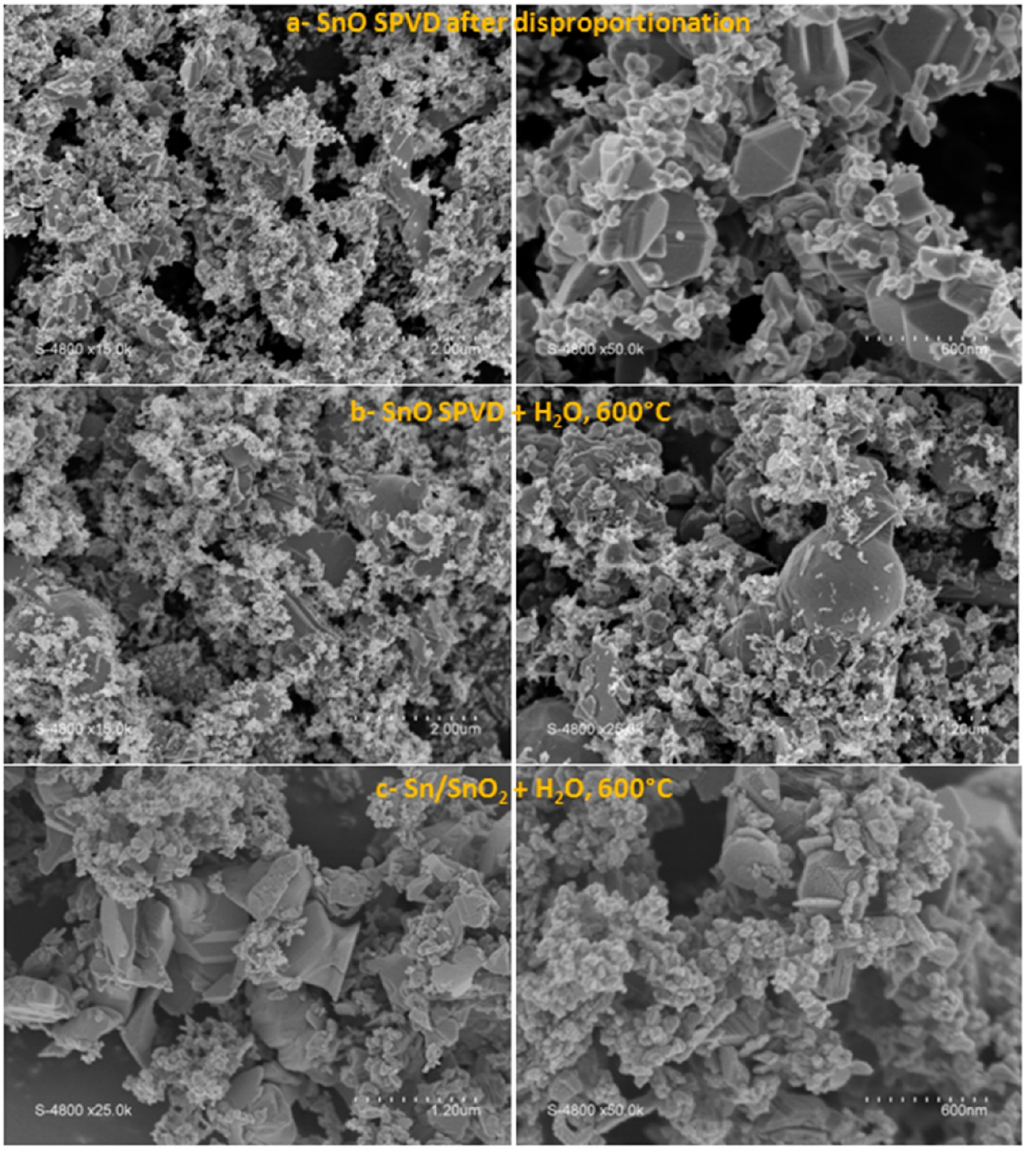

Figure 11. SEM imaging of the tin-based materials: (a) Sn/SnO_2 from disproportionation of SnO SPVD, (b) SnO SPVD after hydrolysis at 600 °C, and (c) Sn/SnO_2 after hydrolysis at 600 °C.

of the gaseous species to the particle surface. However, scanning electron microscopy (SEM) did not reveal the complete covering of the tin particle surface by SnO_2 particles (see section 3.3). Then, the presence of SnO_2 should not disturb the access of the gas to the tin surface. Moreover, the formation of SnO_2 also prevents the conglomeration of tin droplets that would spoil the reactivity.

3.2. Kinetics of the Oxidation Reaction. The kinetic rate of the Sn oxidation reaction can be expressed as[21]

$$r = \frac{d\alpha}{dt} = k_0 \exp\left(\frac{-E_a}{RT}\right)\cdot[y_{ox}]^m \cdot f(\alpha) \quad (4)$$

where α stands for the chemical conversion, k_0 the pre-exponential factor in the Arrhenius relation, E_a the activation energy, R the ideal gas constant, $[y_{ox}]$ the molar fraction of the oxidant gas, m the reaction order relative to the oxidant, and $f(\alpha)$ a term depending on the reaction mechanism. Assuming an excess of oxidant and a zero order reaction, a plot of $\ln(r)$ versus $1/RT$ should give rise to a linear relation, with E_a as the slope. The method was applied to the peak reaction rate obtained during the isothermal runs (Figures 4 and 5), yielding an apparent activation energy of 101 ± 10 kJ mol^{-1} (R^2 = 0.979) for Sn oxidation with CO_2 and 53 ± 1 kJ mol^{-1} (R^2 = 0.999) for Sn oxidation with H_2O (Figure 7). These results related to Sn oxidation are similar to previously reported values for thermally reduced SnO_2 (E_a = 88 ± 7 kJ mol^{-1} for SnO + CO_2 and E_a = 51 ± 7 kJ mol^{-1} for SnO + H_2O).[21] This may be due to SnO disproportionation that presumably occurred in the considered temperature ranges (especially above 650 °C).

In order to investigate the reaction mechanism, the master plot analysis technique[22] was applied to compare the experimental normalized rate data with various model functions corresponding to various solid-state reaction models. The following normalized rate expression was used to compare the results from isothermal runs with common reaction mechanisms. The considered models are summed up in Table 1.

$$\frac{f(\alpha)}{f(A)} = \frac{\frac{d\alpha}{dt}}{\left.\frac{d\alpha}{dt}\right|_{\alpha=A}} \times \frac{\exp\left(\frac{E}{RT}\right)}{\exp\left(\frac{E}{RT}_{\alpha=A}\right)} \quad (5)$$

dx.doi.org/10.1021/ie500206u | Ind. Eng. Chem. Res. XXXX, XXX, XXX−XXX

For high temperature TG runs (Sn/SnO_2 and SnO oxidation with CO_2 at 800 °C), in agreement with ref 21, it is not possible to clearly discriminate between R2 and F1 (Figure 8). Concerning the temperature range corresponding to SnO disproportionation (Figure 9), the experimental data fairly agree with a diffusion mechanism for conversion below 0.25. For larger reaction extent ($\alpha > 0.25$), the F1 model is suitable to describe the reaction mechanism at 550 and 650 °C, whereas the diffusion model seems more adequate at 600 °C. These mechanisms are in accordance with the experimental results that show the most pronounced decrease of the SnO oxidation rate occurring at 600 °C, suggesting a diffusion-controlled mechanism at this temperature.

Hints of explanation may be derived from tin oxides surface characterization although realized under much different conditions (lower temperature). While adsorption of hydroxyl groups on SnO_2 stoichiometric and reduced surfaces was reported, chemisorption of CO_2 in a metastable form and interaction with lattice oxygen was observed.[23] The first mechanism is more prone to the constitution of a passivating layer leading to diffusion limitation. It can be noted that water adsorption depends strongly on the oxidation state of Sn (transformation from a valence of IV to II leads to the formation of a Sn 5s lone pair that is fairly inactive), which may explain the uncertainty on the prevailing reaction mechanism.

The following statements can finally be formulated based on the kinetic analysis of tin species oxidation. Nonisothermal runs show that the oxidation reaction of Sn/SnO_2 with H_2O is slower than with CO_2. Although the reaction with H_2O starts at a lower temperature, the complete conversion is reached earlier with CO_2. Regarding SnO oxidation, a change in the reaction rate is observed around 650 °C, which is likely to be the result of a change in the reactant composition caused by its disproportionation (shift of the main reacting species from SnO to Sn at about 650 °C).

Isothermal runs concerning SnO oxidation between 550 and 650 °C confirm this statement for both H_2O and CO_2: the reaction rate at 600 °C is indeed higher initially than at 550 °C, but it then decreases faster and the final conversion remains lower at 600 °C compared to the other investigated temperatures (550 and 650 °C). This evidences the modification of the reacting species, because of the concomitant disproportionation reaction.

Finally, the kinetic analysis of Sn/SnO_2 oxidation indicates a diffusion-controlled mechanism for reaction with H_2O especially at 600 °C that is not observed with CO_2 at higher temperatures, which may explain the clear linear trend obtained during a nonisothermal run.

3.3. Materials Characterization. SEM imaging (Hitachi S4800) of the synthesized powders shows heterogeneous micronic agglomerates of nanoparticles (Figure 10a,b), containing a lot of interstitial spaces and void fraction favoring internal gas diffusion. The SnO powder consists of disk-shaped SnO particles of different sizes (circular foils of about 0.1 to 1 μm diameter and 50-nm-thick, Figure 10c,d) and nano-entities, as already observed previously.[8] These circular structures disappear after SnO disproportionation and Sn particles (around 100–600 nm) are formed, some of them featuring a nanostructured octahedral shape (Figure 11a). SEM analysis of the disproportionated samples also shows the presence of distinct Sn and SnO_2 particles (Figure 11a). The larger size of the Sn particles compared to the SnO_2 particles supports the existence of tin melting with the resulting particle growth. After hydrolysis at 600 °C (Figure 11b), the morphology of the powder remains similar but with the apparition of some cracks on the SnO disks and the formation of micrometer-size particles (some with spherical shape) that can be attributed to the formation of Sn droplets. For Sn/SnO_2 hydrolysis, the apparition of surface roughness due to Sn oxidation can be noticed (Figure 11c).

XRD analysis of the commercial SnO and SnO SPVD shows that only SnO can be identified on the XRD pattern (Figure 12,

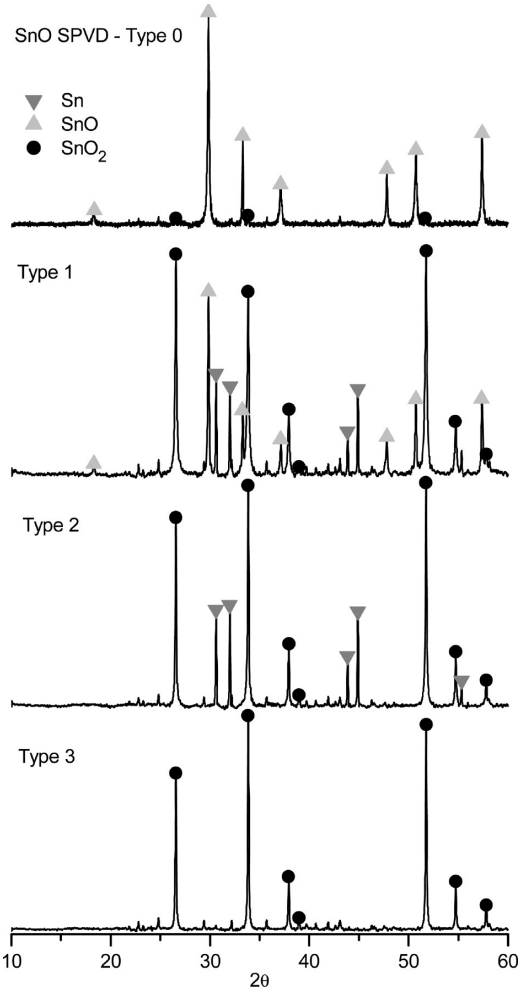

Figure 12. Normalized XRD patterns of the tin-based materials.

Type 0) and the presence of SnO_2 is not detected (it should be in amorphous phase if present). The powder obtained from SnO_2 solar thermal reduction also presents a large predominance of SnO. The powders obtained after oxidation of SnO or Sn/SnO_2 present three main types of XRD patterns. For incomplete reactions with CO_2 at 550 and 600 °C, patterns corresponding to Sn, SnO, and SnO_2 species are identified (Figure 12, Type 1); at higher temperatures, only Sn and SnO_2 remain (SnO + CO_2 at 650 °C, or Sn/SnO_2; Figure 12, Type 2). Incomplete reaction at 550 °C with water presents the same type of diffractogram (Type 2, although only small quantities of Sn are observed), meaning that SnO is preferably oxidized over Sn, and that the disproportionation reaction already takes place at this temperature at a low rate. At a higher temperature with CO_2, for complete reactions with water or for the nonisothermal runs, the final reaction product consists of SnO_2 as the only identifiable pattern (Figure 12, Type 3).

dx.doi.org/10.1021/ie500206u | Ind. Eng. Chem. Res. XXXX, XXX, XXX–XXX

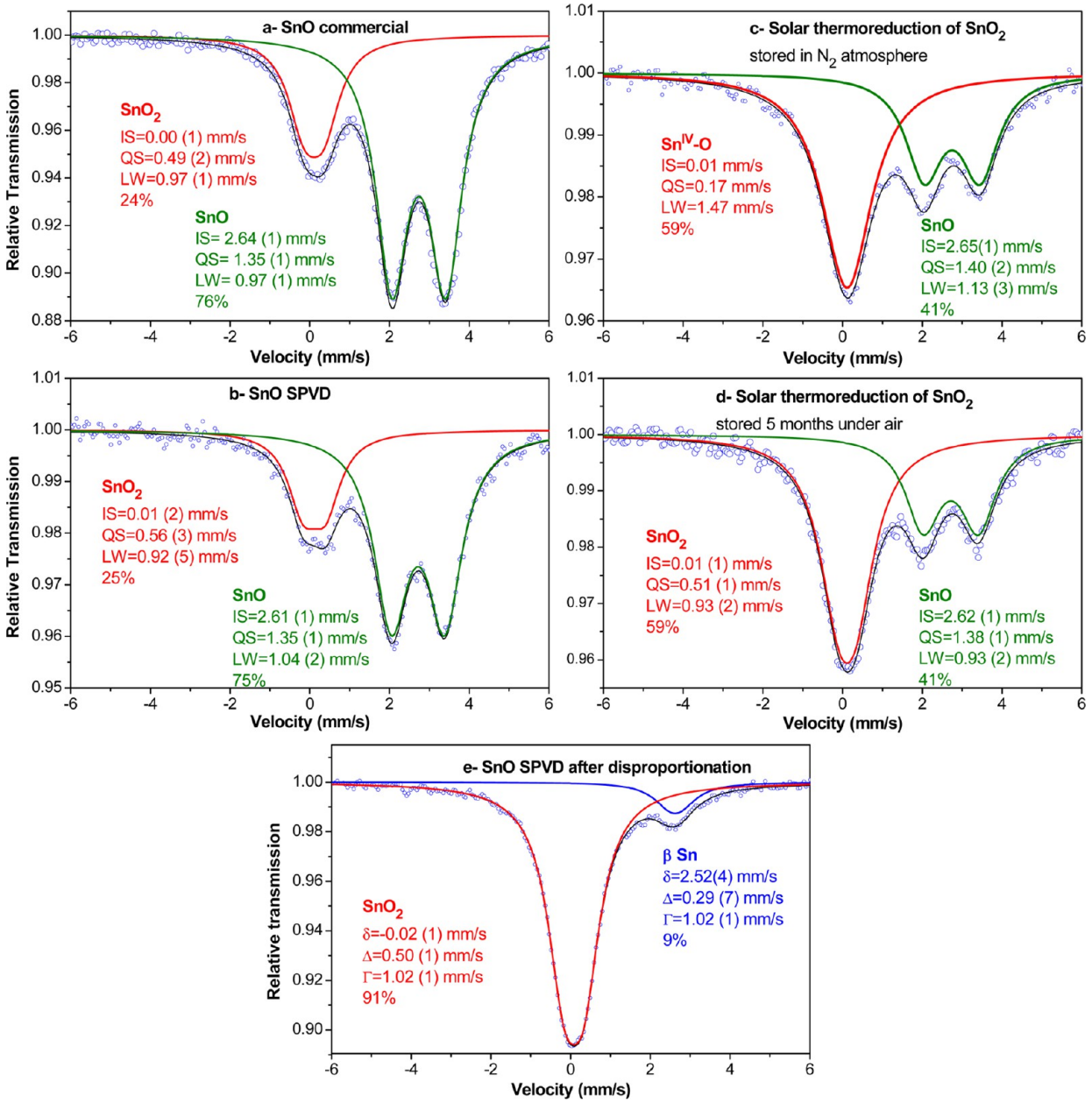

Figure 13. Mössbauer spectra of the source materials. Percentages refer to integral area but not to chemical composition.

Apart from incomplete reactions with CO_2 at 550 and 600 °C (Type 1), an inversion of the main diffraction peak can be observed for Sn, SnO, and SnO_2, as a consequence of a crystal growth favored along the (211) plan instead of (110) for SnO and SnO_2, and along (200) instead of (101) for Sn. This may be related to the morphology shift observed in SEM pictures (Figure 11). The recurrent parasite peaks that can be observed on the various diffractograms are due to the sample holder.

Since the disproportionation reaction takes place at a temperature above the Sn melting point, further characterization of the powders was performed using the BET specific surface area technique, showing a decrease from 18.8 $m^2\ g^{-1}$ before disproportionation to 6.8 $m^2\ g^{-1}$ after, and in either case no microporous volume was detected using the "t-plot" method. Thus, considering that powders are constituted of small spherical particles, a mean equivalent particle size can be evaluated, yielding a diameter of about 54 nm before and 144 nm after disproportionation that corroborates crystallite size evolution. Thus, despite sintering and melting of Sn probably having occurred, complete droplet agglomeration did not take place, and the particle size was not drastically increased because the concomitant SnO_2 formation prevents the conglomeration of tin droplets. Thus, coarsening and tin metal phase segregation did not occur significantly during thermal treatment. This means that the metallic tin phase was evenly dispersed in the powdered material as individual particles, which is also supported by the SEM observations (Figure 11a). The difference in the materials reactivity induced by disproportionation is thus more likely due to a difference in chemical composition than to drastic change in morphology.

3.4. Mössbauer Characterization of the Samples.

Mössbauer characterization reveals that commercial SnO contains 20% mol of SnO_2 (Figure 13a). This composition has been evaluated from the contribution of the Mössbauer subspectra taking into account the different values of Lamb–Mössbauer factors ($f_{SnO_2} = 0.47$ and $f_{SnO} = 0.35$). This corresponds

dx.doi.org/10.1021/ie500206u | Ind. Eng. Chem. Res. XXXX, XXX, XXX−XXX

approximately to the announced purity of the reactant (batch analysis provided by Sigma-Aldrich: 85.7% mass of Sn or 44.7% mol, corresponding to 76% mol of SnO and 24% mol of SnO_2, or 74% mass of SnO and 26% mass of SnO_2). This also agrees closely with the results obtained from complete SnO oxidation in thermogravimetry; i.e., commercial SnO is not pure. Thus, the SnO_2 contained in the reactant must be found as an amorphous phase since it is not detected by XRD analysis. The SnO/SnO_2 composition does not evolve during the SPVD treatment, and the same composition is obtained in the SnO nanopowder (Figure 13b), while only SnO should sublime and be retrieved in the filter (SnO_2 cannot be volatilized without decomposition). This can be due to partial reoxidation after reaction (unlikely since the same composition is obtained for samples collected and stored under a neutral atmosphere) or to a thermolysis of the SnO_2 present in the powder subjected to the direct solar radiation followed by its recombination. The solar thermal reduction of SnO_2 produces a particular Sn^{IV} phase (Figure 13c) that evolves into a "standard" long-term stable Sn^{IV} phase (SnO_2) under an air atmosphere (Figure 13d). The influence of this particular phase on SnO reactivity has not been checked because of its metastable state that evolves rapidly. Complete disproportionation of SnO SPVD is confirmed from TMS (Figure 13e). Finally, incomplete SnO oxidation under CO_2 points out a start of the disproportionation reaction around 600 °C (Figure 14). Indeed, only the Sn^{II} phase is detected after 2 h of SnO oxidation at 550 °C and only βSn is present at 650 °C (in addition to Sn^{IV} that is always detected). At 600 °C, the Mössbauer spectrum is similar to the Sn^{II} spectrum, but with differences in isomer shift and quadrupole splitting. Since the corresponding diffractogram (type 1) contains Sn, SnO, and SnO_2, deconvolution of the spectrum into the corresponding individual curves was tempted but without success (it may be due to the large predominance of Sn^{IV} spectrum). The spectrum of the reaction product at 600 °C may correspond to a metastable intermediate Sn_xO_y-type species, different from previously observed intermediate Sn_3O_4 species.[19] At 650 °C, the composition of the resulting materials can be evaluated from the TMS spectrum as 64% mol of SnO_2 and 36% mol of Sn. These values are in agreement with the presence of about 20% mol of SnO_2 in the starting material (SnO SPVD).

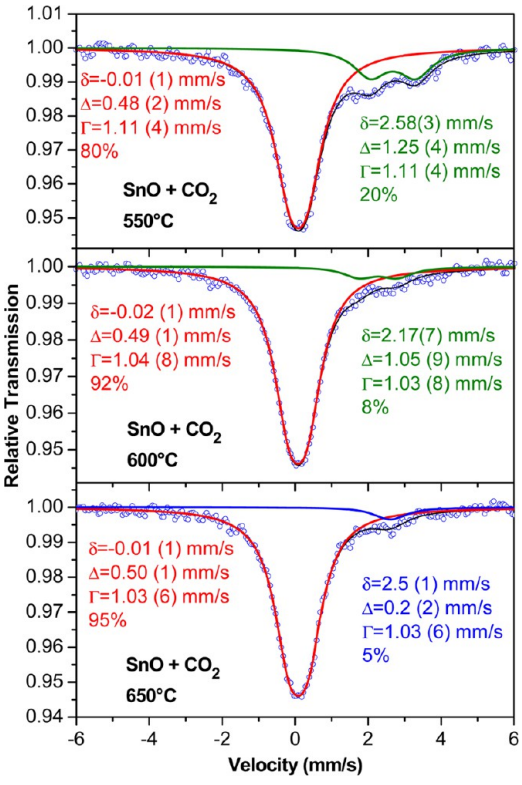

Figure 14. Mössbauer spectra of products from incomplete reactions of SnO with CO_2 at 550 °C, 600 °C, and 650 °C. Percentages refer to integral area but not to chemical composition.

4. CONCLUSION

The oxidation of tin-based species by H_2O and CO_2 for thermochemical fuel production was characterized. The activity of SnO and Sn/SnO_2 with H_2O is much higher than with CO_2 at a given temperature in the range of 550−650 °C. The oxidation of SnO nanopowder obtained via solar sublimation and vapor condensation of commercial SnO (SPVD) shows a higher initial reaction rate at 600 °C than at 550 or 650 °C (for instance, 45% conversion is reached after 15 min versus <35%, during the H_2O reduction reaction), but the reaction slows down after 15 min until reaching a lower rate compared to that measured at 550 or 650 °C for both H_2O and CO_2. This phenomenon has also been observed for SnO obtained from solar thermal reduction of SnO_2. The powder obtained after these reactions at 600 °C contains a particular Sn^{II} phase, presumably more reactive with H_2O and CO_2. This temperature marks the start of a significant disproportionation reaction. At a temperature of 800 °C, SnO is fully disproportionated and Sn oxidation reaches completion. Consequently, tin melting does not lead to powder agglomeration that may hinder the oxidation reaction. The oxidation rate of Sn nanopowder with H_2O and CO_2 is also lower than the oxidation rate of SnO with a similar morphology. The difference in powders reactivity cannot be ascribed to morphology change since the particle size and the specific surface area were not substantially altered after the oxidation reaction, as they remained in the same order of magnitude (no droplets agglomeration was observed). The oxidation rate of the different phases can be hierarchized as follows: Sn^{II} > SnO > Sn. The simultaneous splitting of H_2O and CO_2 is not favorable given the higher reactivity of tin species with H_2O than with CO_2. The splitting of CO_2 requires significantly higher temperatures (800 °C) to reach complete particle conversion. Since the intrinsic activity of metallic Sn during oxidation with H_2O and CO_2 is lower than that of SnO, the efficiency of the fuel production step should be improved by using rapid heating rates to limit the disproportionation reaction and to maximize the amount of reacting Sn^{II} species.

AUTHOR INFORMATION

Corresponding Author

*Tel.: +33 4 68 30 77 30. Fax: +33 4 68 30 77 99. E-mail: stephane.abanades@promes.cnrs.fr.

Notes

The authors declare no competing financial interest.

ACKNOWLEDGMENTS

This study was funded by the energy program of INSIS department of CNRS and by EADS foundation (CNRS CT 084210). The authors also thank E. Bêche and D. Perarnau for XRD characterization.

REFERENCES

(1) Centi, G.; Perathoner, S. Opportunities and Prospects in the Chemical Recycling of Carbon Dioxide to Fuels. *Catal. Today* **2009**, *148*, 191.

(2) Izumi, Y. Recent Advances in the Photocatalytic Conversion of Carbon Dioxide to Fuels with Water And/or Hydrogen Using Solar Energy and beyond. *Coord. Chem. Rev.* **2013**, *257*, 171.

(3) Abanades, S.; Charvin, P.; Flamant, G.; Neveu, P. Screening of Water-Splitting Thermochemical Cycles Potentially Attractive for Hydrogen Production by Concentrated Solar Energy. *Energy* **2006**, *31*, 2805.

(4) D'Souza, L. Thermochemical Hydrogen Production from Water Using Reducible Oxide Materials: A Critical Review. *Mater. Renew. Sustain. Energy* **2013**, *2*, 7.

(5) Abanades, S.; Charvin, P.; Flamant, G.; Lemort, F. Production d'hydrogène par dissociation de l'eau en présence de SnO en utilisant le couple SnO_2/SnO dans une suite de réactions thermochimiques. WO 2008113944, 2007.

(6) Abanades, S.; Charvin, P.; Lemont, F.; Flamant, G. Novel Two-Step SnO_2/SnO Water-Splitting Cycle for Solar Thermochemical Production of Hydrogen. *Int. J. Hydrogen Energy* **2008**, *33*, 6021.

(7) Charvin, P.; Abanades, S.; Lemont, F.; Flamant, G. Experimental Study of SnO_2/SnO/Sn Thermochemical Systems for Solar Production of Hydrogen. *AIChE J.* **2008**, *54*, 2759.

(8) Chambon, M.; Abanades, S.; Flamant, G. Kinetic Investigation of Hydrogen Generation from Hydrolysis of SnO and Zn Solar Nanopowders. *Int. J. Hydrogen Energy* **2009**, *34*, 5326.

(9) Chambon, M.; Abanades, S.; Flamant, G. Thermal Dissociation of Compressed ZnO and SnO_2 Powders in a Moving-Front Solar Thermochemical Reactor. *AIChE J.* **2011**, *57*, 2264.

(10) Levêque, G.; Abanades, S. Kinetic Analysis of High-Temperature Solid−gas Reactions by an Inverse Method Applied to ZnO and SnO_2 Solar Thermal Dissociation. *Chem. Eng. J.* **2013**, *217*, 139.

(11) Stamatiou, A.; Loutzenhiser, P. G.; Steinfeld, A. Solar syngas production via H_2O/CO_2-Splitting thermochemical cycles with Zn/ZnO and FeO/Fe_3O_4 redox reactions. *Chem. Mater.* **2010**, *22*, 851.

(12) Abanades, S.; Chambon, M. CO_2 dissociation and upgrading from 2-step solar thermochemical processes based on ZnO/Zn and SnO_2/SnO redox pairs. *Energy Fuels* **2010**, *24* (12), 6667.

(13) Chambon, M.; Abanades, S.; Flamant, G. Solar Thermal Reduction of ZnO and SnO_2: Characterization of the Recombination Reaction with O2. *Chem. Eng. Sci.* **2010**, *65*, 3671.

(14) Luxmann, L.; Dobner, R. *Metall (Berlin)* **1980**, *34*, 821.

(15) Murken, G.; Trömel, M. Uber Das Bei Der Disproportionierung von SnO Entstehende Zinnoxid, Sn_2O_3. *Z. Anorg. Allg. Chem.* **1973**, *397*, 117.

(16) Giefers, H.; Porsch, F.; Wortmann, G. Kinetics of the Disproportionation of SnO. *Solid State Ionics* **2005**, *176*, 199.

(17) Lawson, F. Tin Oxide—Sn_3O_4. *Nature* **1967**, *215*, 955.

(18) Gauzzi, F.; Verdini, B.; Maddalena, A.; Principi, G. X-Ray Diffraction and Mössbauer Analyses of SnO Disproportionation Products. *Inorg. Chim. Acta* **1985**, *104*, 1.

(19) Moreno, M. S.; Punte, G.; Rigotti, G.; Mercader, R. C.; Weisz, A. D.; Blesa, M. A. Kinetic Study of the Disproportionation of Tin Monoxide. *Solid State Ionics* **2001**, *144*, 81.

(20) Machado-Bailly, C.; Delalu, H.; Létoffé, J. M.; Metz, R. Études Cinétiques de La Dismutation Du Monoxyde D'étain SnO. *J. Phys. IV* **2004**, *113*, 135−138.

(21) Abanades, S. CO_2 and H_2O Reduction by Solar Thermochemical Looping Using SnO_2/SnO Redox Reactions: Thermogravimetric Analysis. *Int. J. Hydrogen Energy* **2012**, *37*, 8223.

(22) Gotor, F. J.; Criado, J. M.; Malek, J.; Koga, N. Kinetic Analysis of Solid-State Reactions: The Universality of Master Plots for Analyzing Isothermal and Nonisothermal Experiments. *J. Phys. Chem. A* **2000**, *104*, 10777.

(23) Batzill, M.; Diebold, U. The Surface and Materials Science of Tin Oxide. *Prog. Surf. Sci.* **2005**, *79*, 47.